Analytical Methods

ROYAL SOCIETY OF CHEMISTRY

CRITICAL REVIEW

View Article Online
View Journal | View Issue

Cite this: *Anal. Methods*, 2025, **17**, 1683

A review of uranium (U) elemental detection methods

Xiang Yu, *[abc] Xuebin Su,*[bc] Zhe Wang,[a] Zongyu Hou[a] and Boping Li[bd]

With the increasing demand for energy, nuclear energy has been developing rapidly. The quantitative detection and qualitative identification of uranium (U) are of great significance for the comprehensive and efficient use of U resources and the control of nuclear and radioactive substances. In this study, the detection of U is divided into liquid sample detection, solid sample detection, gas sample detection, and industrial detection from the perspectives of the sample state and detection environment. For liquid samples, the advantages and disadvantages of various detection methods are summarized. The application of different detection methods for different samples is also analyzed. For solid samples, the application of laser-induced breakdown spectroscopy and X-ray fluorescence in powder compaction and U-containing solid samples is presented. The problems of low instrumental resolution and poor accuracy of quantitative analyses are discussed, and methods to solve the above problems are proposed. For gas samples, UF_6 can be analyzed for U isotopes using laser-induced breakdown spectroscopy. U abundance ($^{235}U/(^{235}U + {}^{238}U)$) is obtained quickly, directly and without the need for sample preparation. Finally, the application of remote detection and *in situ* detection techniques in industrial detection of U is also discussed in this study. In the future, rapid, high-precision and portable U detection methods can be developed by coupling multiple detection methods to meet the needs of different scenarios.

Received 21st November 2024
Accepted 3rd January 2025

DOI: 10.1039/d4ay02115k

rsc.li/methods

1. Introduction

With the growth of population and the development of society, there is a huge demand for basic energy to secure people's livelihoods, and the problem of energy shortage has become a matter of close concern for governments. Considering environmental protection and green development, traditional energy supply can no longer meet the growing energy needs of the people. As a clean energy source, nuclear energy has the advantages of high energy efficiency, low carbon emission and large-scale applicability, which can effectively reduce the emission of greenhouse gases and ease the pressure on energy supply.[1] Uranium (U), as a fissile material, absorbs slow-moving thermal neutrons to undergo nuclear fission, and is the raw material for nuclear power generation. U is widely found in the Earth's crust and oceans.[2] U for nuclear power generation can be extracted by industrial enrichment of U ore or seawater.[3] Rapid access to information on U in seawater and ores is important for achieving efficient exploration and extraction of uranium from seawater and U ores. In addition, nuclear power generation is an important representative of nuclear energy development and is now being applied on a large scale. In order to better monitor the working status of nuclear power plant equipment, it's necessary to remotely detect the working equipment of the nuclear power plant. However, the problem of nuclear contamination caused by nuclear leaks can pose a serious threat to human beings and the environment. By testing samples of groundwater and soil near nuclear power plants, it is possible to quickly monitor whether a nuclear leak has occurred, which is important for the prevention of nuclear contamination.

Based on the above scenarios of nuclear energy development, it can be seen that the detection of U is required in a relatively diverse range of environments. In addition to the need for detection in liquid samples such as seawater, groundwater and rivers, solid samples such as U ore and soil also need to be detected. The detection of U also includes remote monitoring of nuclear power plant equipment and online geological surveys in the field. In the detection of U, the sample contains a variety of other elements in addition to U, which can reduce the accuracy of the detection. And since the U element in the sample is a trace element, it can easily be drowned out by noise and background. In addition, U is highly radioactive, causing irreversible damage to the human body and

[a]*State Key Laboratory of Power System Operation and Control, Tsinghua-Rio Tinto Joint Research Centre for Resources, Energy and Sustainable Development, International Joint Laboratory on Low Carbon Clean Energy Innovation, Institute for Carbon Neutrality, Department of Energy and Power Engineering, Tsinghua University, Beijing, 100084, China*

[b]*National Key Laboratory of Uranium Resources Exploration-Mining and Nuclear Remote Sensing, Beijing, 100029, China. E-mail: yuxiang219@126.com; suxuebin1968@163.com*

[c]*China National Uranium Corporation, Beijing, 100013, China*

[d]*Beijing Research Institute of Uranium Geology, Beijing 100029, China*

the environment.[4] As the exposure distance decreases, its radiation dose increases rapidly, causing even more damage to the human body. Therefore, the detection of U is characterized by high complexity and risk.

The quantitative detection and qualitative identification of U are of great significance for the comprehensive and efficient use of U resources and the control of nuclear and radioactive substances. In the last century, W. Davies and W. Gray proposed the Davies & Grey titration method for the determination of U content by titration.[5] This method is based on the redox nature of U, which can be reduced from the hexavalent state to the tetravalent state, and then its content can be indirectly determined by titration with high precision.[6,7] The method of U detection by titration has some drawbacks, including being time-consuming and labor-intensive, with high operational technical requirements and strict requirements for the experimental environment. More rapid, accurate and convenient analytical methods have been developed in modern times, including inductively coupled plasma optical emission spectroscopy (ICP-OES), inductively coupled plasma mass spectrometry (ICP-MS), ambient ionization mass spectrometry (AIMS), spectrophotometry, fluorescence, atomic absorption spectroscopy (AAS), laser-induced breakdown spectroscopy (LIBS) and X-ray fluorescence (XRF). These methods are widely used in geological exploration, agriculture, food safety, health care and other fields for the detection of U. Among them, ICP-OES, ICP-MS, AIMS, spectrophotometry and AAS have higher detection accuracy and can achieve accurate detection of U. However, the test sample state for these methods is liquid only. If the sample is solid, it needs to be digested, which is a complex and time-consuming process. In recent years, LIBS and XRF have gradually been taken into account. These two methods have the advantages of being fast, convenient and requiring no sample treatment.[8–11] For samples containing U in different states, these two methods can perform highly accurate measurements and avoid complex digestion processes.

In this review, the focus is on the different states of U-containing samples and the detection environment. Based on the different states of the samples and the detection environment, the detection methods can be categorized as U detection with liquid samples, U detection with solid samples, U detection with gas samples, industrial detection of U. The organization of this review is as follows: Section 1 provides the general introduction of U detection; Section 2 introduces U detection with liquid samples; Section 3 introduces U detection with solid samples; Section 4 introduces U detection with gas samples; Section 5 focuses on industrial detection of U. Finally, the future development of U detection methods is discussed.

2. U detection with liquid samples

Detection of U-containing solutions has a wide range of applications in the nuclear industry, environmental monitoring, medical diagnostics and other fields. U detection with liquid samples is a very critical aspect of U detection. In practical applications, the U-containing liquids to be detected come from a wide range of sources, which can be divided into original liquid samples as well as liquids obtained after digestion or rinsing of solid samples. Groundwater, drinking water, seawater, plasma, uranyl liquids and other samples can be regarded as the original samples of U-containing liquids. On the other hand, the liquids obtained from ore samples, soil samples and moss samples after acid digestion belong to the liquids formed after the digestion or transfer of U-containing solid samples. ICP-OES, ICP-MS, AIMS, spectrophotometry, fluorescence, AAS, LIBS, XRF and other detection methods can be used to detect liquid samples. Therefore, the detection of liquids containing U is the most widely studied.

2.1. U-containing solutions

By measuring the original sample as a liquid, it is possible to obtain the content of U in the liquid, from which it is possible to determine whether nuclear contamination has occurred in groundwater or rivers. In addition, the adsorption of U by different adsorption materials and over different adsorption times can be achieved by the detection of the liquid at regular intervals.

ICP-OES detects elements by measuring the intensity of light emitted by excited atoms in an inductively coupled plasma.[12,13] Rezaee and Khalilian proposed a homogeneous liquid–liquid microextraction-assisted ICP-OES method to detect low-content U in liquid samples, and the limit of detection (LOD) and relative standard deviation of detection were 0.4 μg L^{-1} and 6.6%, respectively.[14]

ICP-MS detects elements by measuring the mass-to-charge ratio of ions generated from a sample when it is ionized in an inductively coupled plasma.[15,16] Aswal *et al.* analyzed U, Cr, Ni, As, Mo, Cd, and Pb in Ganges River water in Uttarakhand, India. Seasonal and spatial variations in the concentrations of potentially toxic elements in Ganges water were observed by ICP-MS. The health risk of toxic elements in Ganges water was evaluated by three indicators: pollution index, hazard factor and carcinogenic risk.[17] Similarly, Arti analyzed 20 groundwater samples collected near the industrial area of Jalandhar city for ^{238}U by ICP-MS. The study showed that U concentrations ranged from 4.96 μg L^{-1} to 38.52 μg L^{-1} with a mean value of 17.0 μg L^{-1}, which is below the drinking water limit set by the World Health Organization.[18]

AIMS is a technique for mass spectrometry analysis of complex mixtures without the need for tedious sample treatment. Its greatest advantage over traditional mass spectrometry methods is that it simplifies the sample preparation process and increases the speed and efficiency of analysis. Mannion *et al.* used matrix-assisted ionization (MAI) to analyze solutions of uranyl nitrate, uranyl chloride, uranyl acetate, and uranyl oxalate. The samples and matrix crystal suspensions were analyzed using an atmospheric pressure time-of-flight mass spectrometer by introducing them into the atmospheric pressure inlet of the mass spectrometer. All four uranyl complexes were detected with a detection time of only a few seconds. The LODs were 5 ng for uranyl nitrate, 10 ng for uranyl oxalate, 100 ng for uranyl chloride and 200 ng for uranyl acetate.[19] Coopersmith *et al.* used paper spray ionization mass spectrometry (PSI-

MS) to analyze solutions containing uranyl acetate, uranyl chloride, uranyl nitrate, and tri-*n*-butyl phosphate uranyl complexes. For the quantitative analysis of U using gadolinium nitrate as an internal standard, the signal-to-noise ratio for UO^{2+} was about 1000 and the acquisition time was about 1 min. For isotopic quantification of U, longer accumulation times (>15 min) can improve precision and reduce errors in secondary ^{235}U isotopic abundance measurements to 1%.[20] Dion *et al.* analyzed nine aqueous solutions of inorganic cations using electrospray ionization-ion mobility spectrometry (ESI-IMS). Different counterbalance ions affected the detection sensitivity and the types of responding ions. The spectra of uranyl acetate and uranyl nitrate showed only one response ion peak. The signal-to-noise ratio (S/N) of uranyl acetate was 41 and the predicted detection limit (PDL) was 0.90 ng L^{-1} at a concentration of 50 ng L^{-1}. The S/N ratio of uranyl nitrate was 6.0 and the PDL was 13 ng L^{-1} at a concentration of 100 ng L^{-1}. The results showed that the detection of uranyl acetate and uranyl nitrate was very sensitive and the detection of uranyl nitrate was very low.[21]

Spectrophotometry detects analytes by measuring the amount of light absorbed or transmitted by a sample at different wavelengths.[22] Behpour *et al.* measured the concentration of U in solution by using spectrophotometry. They used naphthalene-methyltrioctylammonium chloride as a substrate to immobilise arsenazo (III), with which chelates were formed when a U-containing solution flowed through the arsenazo (III). The chelate was then quantitatively eluted with ammonium tetraphenylborate to form the solution to be measured, and U's concentration was obtained by testing the solution to be detected.[23] Mukhopadhyay *et al.* used turbid point extraction of U in spent fuel reprocessing tailings, and then used spectrophotometry to measure the U content in spent fuel samples.[24] Hixon *et al.* used U/TEVA-2 extraction chromatography resin to concentrate U in liquid samples, and then used a color indicator to react with the U concentrate to determine whether the U content in drinking water exceeded the standard.[25] Kumar *et al.* used a UV-visible spectrophotometric method combined with the orthogonal signal correction-assisted principal component regression (OSC-PCR) chemometric method for the simultaneous determination of U and nitric acid.[26]

Fluorescence detects analytes by measuring the light emitted when molecules in the sample return to their ground state after being excited by a specific wavelength of light.[27] Badr *et al.* used a new fluorescent reagent which can selectively enhance the fluorescence at a wavelength of 557 nm. The effects of pH, solvent type, ligand concentration, action time, and interfering ions on the fluorescence detection of U ions were also investigated, with a detection limit of 0.1 ppm.[28] Xiao *et al.* synthesised a new fluorescent covalent organic polymer, which, by using its strong coordination ability with U and excellent fluorescence properties enables better performance in the detection of U in water samples.[29] Kumar *et al.* used a fluorescence method for the detection of U in reactor nuclear grade sodium with a LOD of 0.2 μg g^{-1}.[30] Hidayath *et al.* used a LED fluorometer to detect the fluorescence intensity of aqueous samples at specific wavelengths in conjunction with a calibration of a standard U solution to successfully determined U concentration in groundwater samples from 75 locations in the Davanagere district, Karnataka, India.[31]

AAS detects analytes by measuring the absorption of light at specific wavelengths by the atoms in a sample that have been vaporized and excited in a flame or graphite furnace.[32] Kaur *et al.* used AAS and ICP-MS to examine groundwater in rural areas of southwestern India, and their results showed that the U content in the water exceeded the limit, which would be hazardous to human health.[33] Goyal *et al.* explored the mechanism of atomization of U in the presence of aqueous media and plutonium matrices and determined the U content in plutonium based on Electro-Thermal Atomization Atomic Absorption Spectrometry (ETA-AAS).[34] In order to assess the effect of different metal ions on U adsorption, Smječanin *et al.* measured the elemental U content in the presence of different metal ions using the AAS technique. A new adsorption method is proposed that can absorb U with high efficiency and low cost, and the adsorbent preparation and experimental batch procedure are designed as shown in Fig. 1. It was found that the efficiency of U adsorption decreases in the presence of cobalt, nickel and lead ions.[35]

LIBS uses a high-energy laser to vaporize and excite a small portion of the sample, which then emits characteristic light that is analyzed to determine elemental composition.[36,37] Akpovo *et al.* used a silicon wafer as a substrate and coated it with a dehydrated uranyl solution, eliminating the possibility of confusing the U elemental leaps with the silicon substrate leaps. Analyzing the plasma expansion mechanism, the spectral enhancement effect of a CO_2 laser was compared with that of a femtosecond or nanosecond laser, enhancing the spectral peak area by a factor of about 226.[38] Chinni *et al.* dropped U-containing solutions on aluminum alloy, plastic and ceramic tiles. The experiment demonstrated that the high spectral background intensity is due to the high density of the U emission spectral lines. The decay rate of the U spectral lines can be altered by the introduction of argon to increase the signal-to-background ratio, and the spectral intensity of U is enhanced using a laser double pulse to achieve a surface LOD of 13–150 μg cm^{-2}.[39] Russo *et al.* ingeniously created a special monodispersed microdroplet dispenser to prepare U samples with a known volume and U concentration of the microdroplet samples. The experimental setup is shown in Fig. 2. A linear calibration curve was established for U mass from 6.5 pg to 65 pg, with an R^2 of 0.965 and a LOD of 1.3 pg.[40]

XRF determines the elemental composition of a sample by measuring the fluorescent X-rays emitted when the sample is exposed to high-energy X-rays.[41,42] Li *et al.* used a novel magnetic covalent organic framework material (Fe_3O_4@COF) as an adsorbent in combination with magnetic dispersion solid phase extraction. A rapid adsorption time of 15 min and a LOD of 0.008 μg L^{-1} were achieved without the need for a centrifuge and a filter for the efficient enrichment and on-site determination of trace U.[43] Zhang *et al.* applied the energy dispersive XRF technique for U detection. The optimal parameters including filter material, collimator aperture and detector angle were determined by MCNP simulation, and the effectiveness of

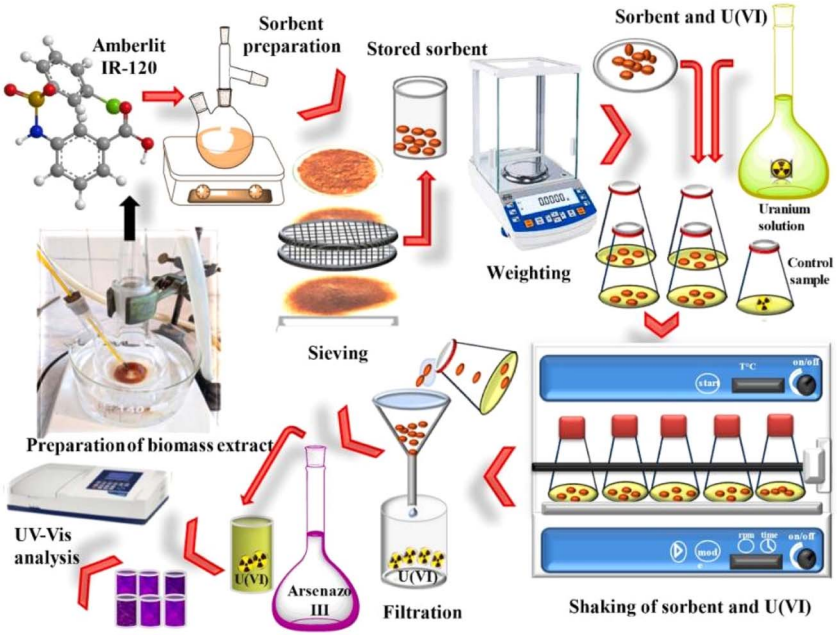

Fig. 1 Schematic overview of sorbent preparation and experimental batch procedure design. Reproduced from ref. 35 with permission from Elsevier, copyright 2025.

this technique for U detection was experimentally verified.[44] In order to overcome the complex sample pre-treatment required for the determination of U content by methods such as alpha spectroscopy, researchers used total reflection X-ray fluorescence spectroscopy (TXRF) to study the detection of U content in wastewater. The matrix interference was eliminated by adding iridium as an internal standard to the effluent and drying the treated sample solution. TXRF was used to detect the dried deposits of the sample solution on an optical glass plate, and the LOD of this method for U content was 0.30 ppm.[45] Izumoto *et al.* used U-containing blood to simulate nuclear-contaminated human blood samples, and then detected the simulated blood samples added dropwise to filter paper using XRF. The schematic of the experimental setup is shown in Fig. 3. The LOD for U concentration in blood samples was improved to 0.45 ppm, which is 1000 times lower than that of commercially available blood U content meters. This method can be used for the rapid detection and evaluation of nuclear radioactive contamination in personnel during nuclear accidents.[46] In order to eliminate the interference of rubidium and potassium elements on the XRF detection of U content in samples, Takahashi *et al.* used graphene oxide as a solid phase to enrich U in water samples. The U-enriched graphene oxide was filtered using a filtration membrane to eliminate the effects of rubidium and potassium in the solution. The U adsorbed on graphene oxide was extracted by nitric acid elution to prepare a solution for measurement, and gallium was added to the solution as an internal standard. Finally, the U content of the sample on the slide was detected by using TXRF, which enables rapid and low LOD for U content in liquid samples.[47] Yoshii *et al.* added graphene oxide nanosheets to a brackish water sample to adsorb the U in the sample, then collected the graphene oxide nanosheets using a membrane filter and analyzed them by XRF. The presence of U contamination in brackish water can be confirmed when the intensity of the U peak is significantly higher than the background U content deduced

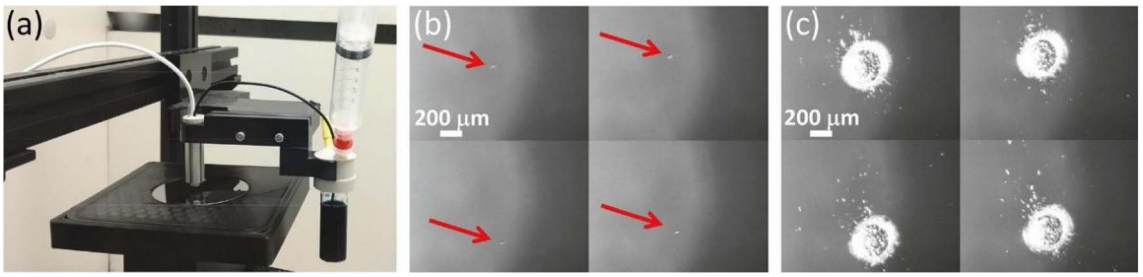

Fig. 2 Photographs of (a) the setup for printing on-demand, single monodispersed droplets onto a Si-wafer substrate with green ink showing the solution reservoir, (b) dried droplets on a Si wafer (see red arrows) before and (c) after LIBS measurement. The Si wafer that appears as a shiny circular disc in the center of the 2D-translation platform measures 5 cm in diameter. Reproduced from ref. 40 with permission from Elsevier, copyright 2025.

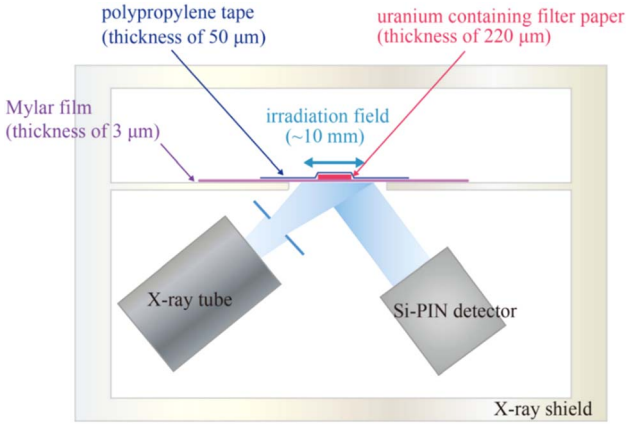

Fig. 3 The schematic of the experimental setup. Although not shown in the figure, two spaces (sample side, X-ray tube and detector side) are partitioned by a 6-μm polypropylene film. Reproduced from ref. 46 with permission from John Wiley and Sons, copyright 2025.

from the salinity value, which is important for environmental monitoring after an accident.[48]

Different detection methods have different limits of detection, advantages and disadvantages. ICP-OES and ICP-MS have high sensitivity and multi-element analysis capability, with a LOD of up to ppb level or even lower, making them suitable for the detection of ultra-low content of U. Spectrophotometry requires chemical reaction and extraction to obtain the U content, which is cumbersome and time-consuming. In fluorescence analysis, the U element itself does not have fluorescence characteristics, so it is necessary to add fluorescence reagents to carry out fluorescence detection. AIMS is still in a developmental stage compared to traditional mass spectrometry techniques. Matrix effects may affect the ionization efficiency and analytical results, which need to be corrected appropriately. And the fluorescence intensity is easily affected by the composition and pH value of the prepared solution to be tested, which leads to certain limitations to the fluorescence method. Although LIBS has the advantages of being fast and convenient, the LOD in U-containing liquids is poor and only reaches the ppm level. For measurements in U-containing liquids, XRF not only has the advantage of speed, but also has the advantage of a low detection limit. Therefore, compared with other detection methods, XRF is more widely used in the measurement of U-containing liquids. In summary, for the detection of U in liquid samples, there exist a variety of detection methods that can be accomplished.

2.2. Solid to liquid preparation

ICP-OES, ICP-MS, AIMS, spectrophotometry, fluorescence, and AAS are not suitable for the direct detection of solid samples because they can detect only liquid samples. These methods require strong acid digestion or buffer rinsing of the solid sample to convert it into a liquid for detection.

Varnava *et al.* compared the leaching efficiency of different leaching solutions of $NaHCO_3$, citric acid and EDTA. The leachate was mixed with phosphogypsum and the mixture was shaken in an oscillating incubator at ambient temperature. Aliquots were obtained after 15, 30 and 45 days respectively. The U concentration in the leachate of phosphogypsum was analyzed using ICP-OES, which effectively tracked the leaching rate of U at different time intervals.[49] Almeshari *et al.* examined U and rare earth elements in soil by ICP-OES. In order to create the digestion solution, a beaker was used to combine HNO_3, H_2O_2, and dry soil. Following a period of 48 h, the digestion mixture was subjected to heating at 79 °C for a duration of 5 h. The resulting solution was then cooled to room temperature, extracted, and filtered. The results explained that the concentration of U in the soil of Ras Tanura ranged from 0.07 to 5.72 mg kg^{-1}, with an average concentration of 3.30 mg kg^{-1}. In addition, it was found that the distribution of U and rare earth elements in the soil of the area was not homogeneous, with some spatial and inter-elemental correlations.[50]

Greene *et al.* used a malonic acid buffer rinse to extract U from the surface of building materials. Then arsenazo (III) was used to form a blue complex with the U in the acidic extraction solution. The LOD of this method for U content on building surfaces was 5 ng cm^{-2}, as determined by spectrophotometry. The absorbance spectra of arsenic-nitrogen III complexes formed by other metal ions commonly found in building materials are shown in Fig. 4.[51]

Borylo *et al.* used AAS to detect the content of U and polonium elements in mosses from the northern part of Poland. The moss was completely dried in a well-ventilated area. The dried moss was digested with concentrated nitric acid and concentrated hydrochloric acid to complete the process of conversion of solid into liquid. It was shown that U and polonium in mosses are mainly due to the deposition of radioactively contaminated air, providing a new method for the evaluation of nuclear radioactive contamination.[52]

Hoegg *et al.* analyzed a series of certified reference materials (CRMs) with increasing concentrations of U using a Liquid Sampling-Atmospheric Pressure Glow Discharge-Orbitrap system (LS-APGD-Orbitrap). Samples were prepared by dissolving U_3O_8 in 8 M HNO_3, then diluting to a concentration of 200 μg mL^{-1} with 1 M HNO_3, and finally further diluting with 2% HNO_3. The LS-APGD-Orbitrap system monitors U isotopes in the form of UO^{2+} ions. The LS-APGD-Orbitrap system performed well in the analysis of highly enriched U samples compared to conventional methods, and was able to measure all U isotopes including ^{234}U and ^{236}U-related species. However, the measurement accuracy of low-abundance isotopes is compromised by the limitations of the automatic background deduction step, which results in large systematic errors.[53]

Bowden *et al.* used matrix-assisted ionization-time-of-flight mass spectrometry (MAI-ToF MS) to analyze U CRMs. Sample solutions were prepared by combining ≈10 mg of 3-NBN, 50 μL of methanol, and U standards in 2% nitric acid to yield a final sample volume of 100 μL. By this method, $^{235}U/^{238}U$ ratios were quantified for CRMs with different concentrations and different isotopic compositions. The method accurately calibrated $^{235}U/^{238}U$ ratios with relative uncertainties ranging from 4.7% to 17.2% (approximately ±95% confidence level) and weighted-mean uncertainty close to 1.5%.[54]

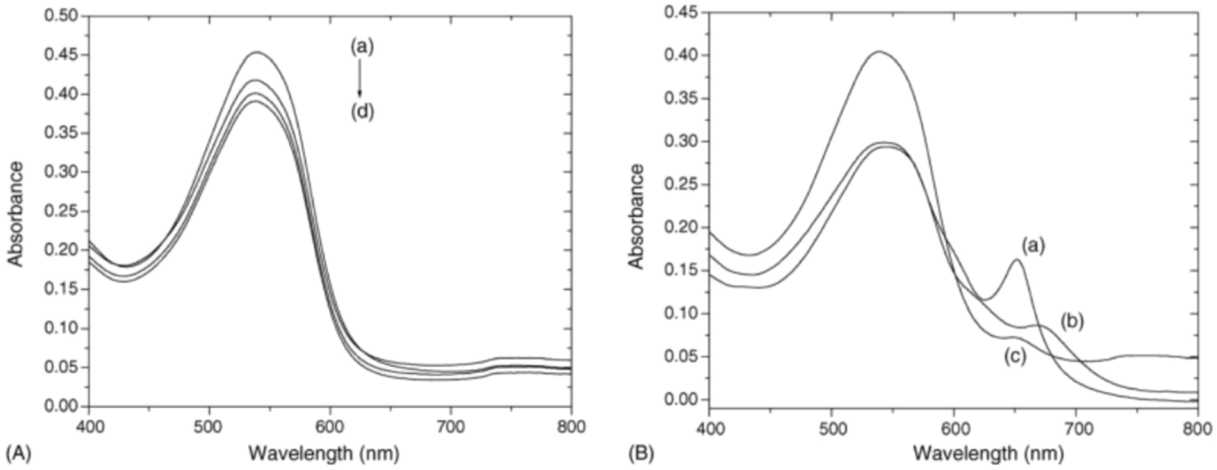

Fig. 4 Absorbance of various cation:arsenazo III complexes after washing of building material surfaces (washed and measured at pH 2.2): (A) calcium (a), magnesium (b), iron (c), and aluminum (d); (B) U (a), thorium (b), and cerium (c). Analyte concentrations: [cation] = 500 μg L^{-1}, [Arsenazo III] = 10 mg L^{-1}. Reproduced from ref. 51 with permission from Elsevier, copyright 2025.

Solid samples can also be analyzed by ICP-OES, spectrophotometry, AAS, and AIMS through sample treatments such as digestion and rinsing. However, the sample treatment for digestion and rinsing is cumbersome and slow, which can take several hours to convert a solid to a liquid. The inability of ICP-OES, ICP-MS, AIMS, spectrophotometry, fluorescence, and AAS to directly detect defects in solid samples is the most important reason why these methods cannot be applied on a large scale in the field of U detection in solid samples.

3. U detection in solid samples

In the detection of solid samples containing U, it is divided into detection of powder compaction and detection without treatment. Powder compaction is the process whereby a standard sample of U is powdered and bonded under high pressure to form a pellet. This method of detection is generally used in laboratory detection. Detection without sample treatment has a wider range of applications. It is capable of detecting U under both laboratory conditions and field conditions.

ICP-OES, ICP-MS, spectrophotometry, fluorescence, and AAS are not suitable for the direct detection of solid samples as the samples are liquids. For the detection of solid samples, LIBS and XRF are the most popular methods, which avoid the need for complex and time-consuming digestion processes. They provide rapid detection of U ore, U-bearing glass, U foils and depleted U metal flakes to obtain accurate information on the U content.

3.1. Powder compaction

Powder compaction is a common method of sample preparation. It involves weighing a certain mass of powder using a balance. By placing the powder sample in a modelling apparatus, high pressure is applied to bind the powder into pellets. The whole process of powder compaction takes less than ten minutes in total. Compared to the digestion process, powder compaction is faster and more efficient, saving a lot of time. Powder compaction improves the homogeneity and signal stability of the sample.

D.A. Galson ground the samples into powder and mixed the homogeneous powder with a few drops of methyl cellulose binder and pressed it into 32 mm diameter samples at a pressure of 2 tones. Rapid measurements of the elemental content of low levels of U, thorium and potassium in silicate rock were made using XRF with absorption correction for U and thorium achieved using Compton scattering intensity, with a LOD of 0.13–0.16 ppm for U.[55]

Ji *et al.* increased the spectral intensity and detection limit of U by improving the laser beam quality of LIBS. The experimental setup and principle are shown in Fig. 5. A new powder concentration was prepared by mixing a certain proportion of silica powder with the existing concentration of powder. The powder of the standard samples was pressed into pellets of diameter 30 mm under a pressure of 25 MPa with flat surfaces. Through a beam shaping mirror, the Gaussian beam with non-uniformly distributed energy is converted into a flat-topped beam with uniformly distributed energy. Mechanistically analyzing the flat-top beam reduces the shielding effect of the plasma, increases the spectral intensity by a factor of 3–6 and reduces the RSD to less than 15%. Based on the principle of signal identification with a signal-to-noise ratio greater than 3, the LOD is roughly estimated to be around 24 ppm.[56] Li *et al.* used LIBS combined with laser-induced fluorescence to excite lower energy level particles of elemental U to the upper energy level. Multiple combinations of excitation and analysis lines are analyzed. The principle is shown in Fig. 6. Four standard samples with different concentrations were proportionally weighed and mixed for 30 minutes using a vortex mixer to obtain powders of different concentrations, which were finally pressed into flat sheet samples at 30 MPa. The spectral intensity was amplified by a factor of 21, with an R^2 of 0.998, a RMSE of 0.05%, and a LOD of 35 μg g^{-1}.[57] Based on the conventional LIBS experimental setup, Zhang *et al.* proposed an optoelectronic double-pulse method to improve the spectral intensity.

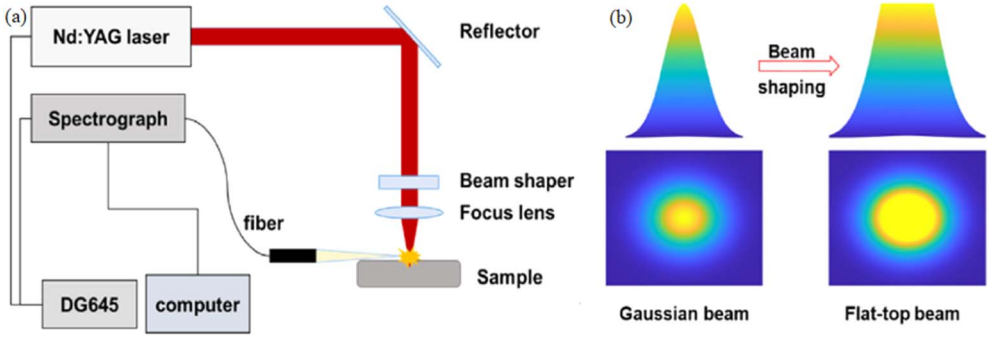

Fig. 5 Gaussian beam rectification into a flat-topped beam to detect U. Reproduced from ref. 56 with permission from Elsevier, copyright 2025.

By optimizing the laser pulse energy, voltage and other parameters, the spectral intensity was enhanced by a maximum of about 10 times, which is much higher than that achieved with the laser double-pulse technique. On the basis of the above experiments and by replacing the soil matrix with a pure silica matrix, the substrate effect of the soil was effectively avoided. R^2, RSD and LOD were improved to 0.997, 5.53%, and 64 μg kg^{-1}, respectively.[58] Manard *et al.* combined LIBS with laser ablation multi-receiver inductively coupled plasma mass spectrometry (LA-MC-ICP-MS) for the simultaneous determination of fluorine content and U isotope ratios in uranyl fluoride particles, which will be useful for the study of phase transitions of UO_2F_2 particles as well as for the identification of nuclear materials and nuclear energy applications.[59]

In LIBS, during the detection of U at LIBS, the spectral lines of U are so dense that it is difficult to obtain effective information. Machine learning algorithms can learn the complex relationship between elemental content and spectral lines from a large amount of data, and discover patterns and laws hidden in the data. By training the model, a non-linear mapping relationship between elemental content and signal intensity can be established to predict the elemental content of unknown samples.[60] Combining LIBS with machine learning algorithms, multiple features of U can be extracted, dramatically improving the accuracy and stability of quantitative analysis.

Han *et al.* prepared salt mixtures by mixing various salts. U content in high-temperature lithium chloride and potassium chloride salts was measured using normalized and partial least squares regression methods, with a limit of detection of 0.0942 wt% and an RMSE of 0.1602.[61] Mao *et al.* combined the LIBS atomic spectral lines of U isotopes with the Laser Ablation Molecular Isotropic Spectrometry (LAMIS) molecular bands. By summing the two U isotope compositions, it is possible to directly simulate the U emission spectra for any desired percentage of ^{235}U and ^{238}U abundance. The accuracy of quantitative analyses was improved by extracting isotope abundance information from LIBS or LAMIS spectra using partial least squares multivariate regression.[62] Fan *et al.* used the standard addition method to add ThO_2 and U_3O_8 powders to graphite powder with 99.9% purity. The quantitative analyses of the three methods including the standard curve method, random forest and partial least squares regression were compared in combination with univariate regression and multivariate regression models. The results of the research showed that partial least squares regression improved the root mean square error and mean relative error of prediction more significantly, while random forests improved the linear correlation coefficient more significantly.[63]

The researchers were able to improve the stability of the signal by pressing the solid powder into flat pellets. By choosing

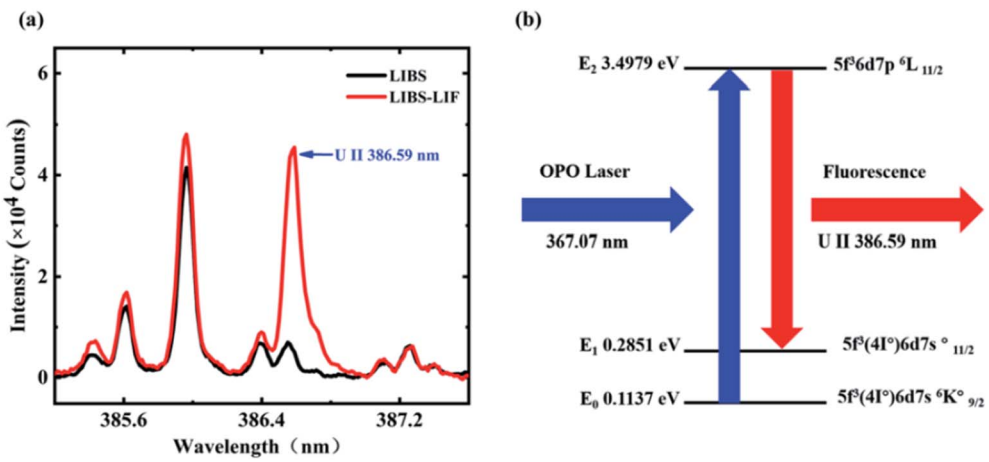

Fig. 6 Principle of LIBS-LIF detection of U. Reproduced from ref. 57 with permission from Royal Society of Chemistry, copyright 2025.

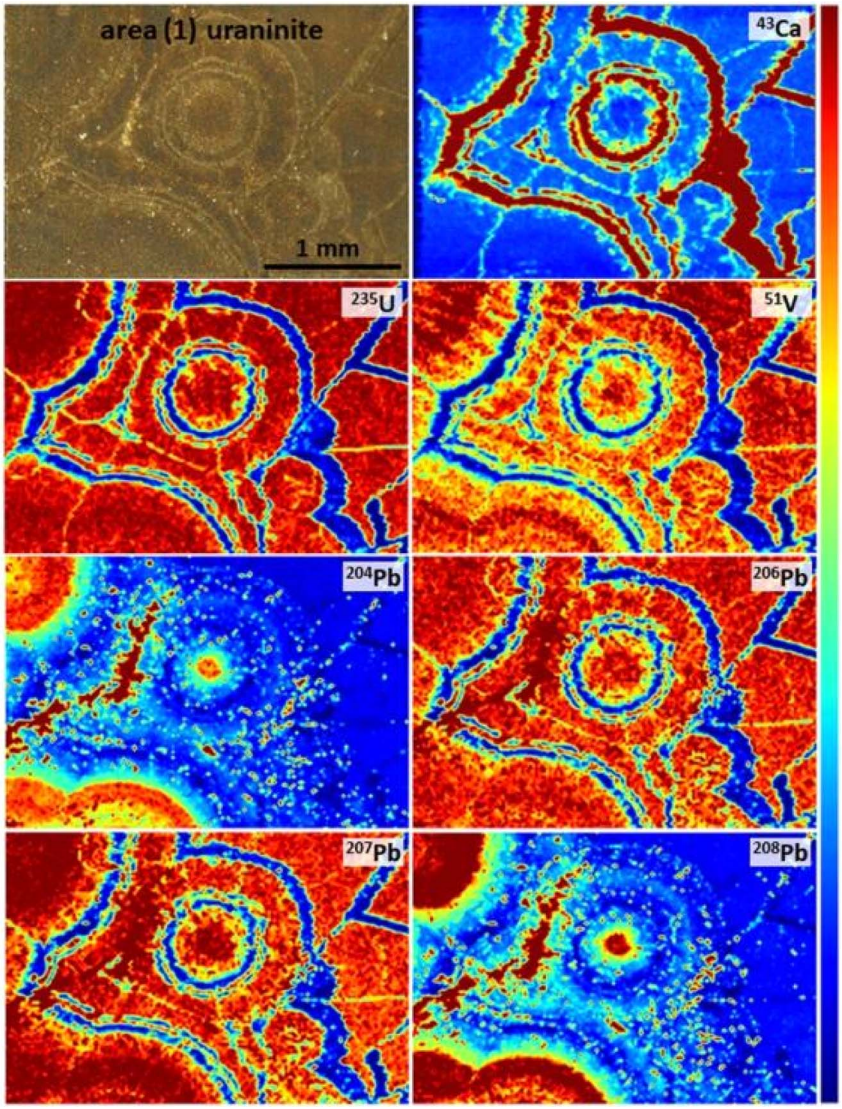

Fig. 7 Photography of the analyzed sample area (1) and distribution of selected isotopes in uraninite obtained by LA-ICP-MS. Normalized intensities in cps, with blue color representing the minimum, red representing the maximum. Reproduced from ref. 69 with permission from Elsevier, copyright 2025.

a suitable substrate, the matrix effect can be effectively avoided. Combining LIBS with machine learning algorithms can significantly improve the accuracy of quantitative analysis and reduce errors. However, mixing powder samples with different concentrations can cause problems of uneven mixing and long mixing time. How to mix the powder quickly and uniformly is an important issue to further improve the stability of the signal and the accuracy of quantitative analysis.

3.2. U-containing solid samples

The direct detection of U-containing ores, glass and metal flakes without sample treatment is negatively affected by matrix effects. Since the samples contain a variety of interfering elements, higher demands are placed on the resolution of the instrument. It is difficult to obtain a high degree of accuracy when quantitatively analyzing samples directly. Improving the resolution of the instrument to obtain the content and distribution of U quickly and accurately is the key to detection without sample treatment.

Adimedha *et al.* used micro-area X-ray fluorescence spectroscopy (Micro-XRF) to map elemental distributions of ores. By analyzing the elemental distribution maps, the elemental composition of the minerals and the exact location and form in which they are located can be determined.[64] In order to reduce the interference of other elemental spectral lines and the baseline on the U spectral lines, Choi *et al.* utilized LIBS combined with an anti-convolution algorithm to reduce the degree of spectral peak overlap by changing the bandwidth of the spectrometer. The plasma evolution process was also analyzed to optimize the delay time based on spectral information such as Stark spreading width to reduce the baseline of U ore and U-bearing glass.[65] Morgan *et al.* used an interferometric hybrid spectrometer to analyze the LIBS spectral characteristics of U isotopes in U foils. The 25 pm isotopic shift of U

in ambient air was resolved at 424.437 nm with a resolution of 6 pm. However, the spectral overlap between U(I) 424.626 nm and U(II) 424.412 nm was not resolved.[66] Zhang *et al.* investigated the LIBS spectra of U metal under different ambient gases and their characteristics. The enhancement mechanism of depleted U metal sheets in ambient gases and the effect of the gas flow rate on the spectra were analyzed by observing the spectral features and the characteristic spectral lines of U in argon, neon, oxygen and nitrogen.[67]

A method to combine LIBS and PIFS (plasma-induced fluorescence spectroscopy) was proposed by Liu *et al.* By adjusting the size of the laser spot, the two techniques, LIBS and PIFS, can be switched. LIBS was used to detect the major elements with higher contents, and PIFS was used to detect U and samarium in zircon glass. R^2 of U and samarium were improved to 0.9478 and 0.9969 with LODs of 154 ppm and 6 ppm, respectively.[68] Holá *et al.* used the technique of LIBS coupled with laser ablation-inductively coupled plasma mass spectrometry (LA-ICP-MS), which reasonably combines the advantages of fast and large-area imaging of LIBS with the advantages of high resolution and low resolution of LA-ICP-MS. Based on the advantages of both techniques, a detailed U distribution can be quickly obtained in the whole sample image. The distribution of isotopes of each element is shown in Fig. 7.[69] Similarly, Andrews *et al.* used a combination of LIBS and LA-ICP-MS for the detection of U in minerals. LIBS was used to rapidly screen the distribution of U in the samples to locate the minerals. The selected locations were then further analyzed using high-resolution LA-ICP-MS to obtain confidence in the U isotopic composition of the U ore. This method significantly reduced the analysis time (~95%) compared to LA-ICP-MS alone.[70]

LIBS and XRF allow the direct detection of U-containing ores, glass and metal flakes without sample treatment, greatly improving detection time and efficiency. Micro-XRF and LIBS coupled with LA-ICP-MS can be used to map the elemental distribution and determine the elemental composition of the ore and its distribution. However, the current detection method without treatment still has some shortcomings. Firstly, due to the presence of multiple interfering elements in the samples, the instrument requires higher resolution to distinguish the U characteristic spectral lines from the interfering signals. Secondly, some researchers have found in their experiments that the detection methods without treatment often face difficulty in obtaining highly accurate quantitative analysis results because the characteristic spectral lines of other elements and the baseline may interfere with the measurement of the U characteristic spectral lines. In order to improve the performance of direct detection of solid samples, further optimization of the resolution of the instrument could be attempted to reduce the influence of interfering elements on the U characteristic spectral lines. More advanced data processing algorithms and techniques could also be explored to improve the accuracy of the U content and distribution. In addition, combining multiple analytical techniques, such as LIBS and XRF or LIBS and LA-ICP-MS, can be considered to compensate for the limitations of a single technique and to improve the comprehensiveness and accuracy of the analyses.

4. U detection with gas samples

U ores have very low grades, especially in terms of the natural abundance of ^{235}U, which is only 0.72%. In order to obtain nuclear pure U, it must undergo a series of enrichment and purification processes. U is enriched by hydrofluorinating U oxide to U tetrafluoride, and then fluorinating U tetrafluoride to uranium hexafluoride (UF_6) – the only known volatile compound of U. By gaseous diffusion and gas centrifugation, ^{235}U and ^{238}U can be separated. Therefore, as the first line of defense against nuclear proliferation, accurate determinations of U enrichment in UF_6 are critical for International Atomic Energy Agency (IAEA)'s material verification, accounting, and safeguards.

Chan *et al.* used LIBS to perform direct measurements of gaseous UF_6 without sample pretreatment. Fig. 8 shows a photograph of the experimental setup. The determination of the U isotopic content of gaseous UF_6 was accomplished by investigating the spectral characteristics of the U II 424.437 nm spectral line and its isotopic shifts, the evolution of the signal and background, and the variation of the Stark widths and shifts with the pressure of the UF_6 gas and the energy of the nanosecond Nd:YAG laser pulses. It was found that the LIBS spectra of gaseous UF_6 at low laser energies and pressures were similar to those of solid U samples. However, when using the ^{235}U–^{238}U line pair at 424.412–424.437 nm for UF_6 enrichment analysis, there is a systematic positive bias, which was confirmed to be caused by self-absorption. Even if a self-absorption term is included in the spectral fitting algorithm to compensate for self-absorption, it remains a major limiting factor in the accuracy of UF_6 enrichment analysis.[71] To solve the problem of self-absorption in atomic emission lines, they chose a new spectral window (centered at 421.3 nm) that contains a series of U atomic emission lines with significant ^{235}U–^{238}U isotopic shifts that are not susceptible to self-absorption. The effect of outliers was minimized by introducing a wavelength-dependent weighting factor based on the position of the spectral lines. In addition, the determined isotope ratios were then inversely introduced into the weighting factor to compensate for the inhomogeneous uncertainty distribution of the data points. Finally, an isotope-shift-based weighting factor was added to highlight the contribution of the emission lines with large isotope shifts to the enrichment determination. As a result of these improvements, the algorithm achieved mean absolute deviations within 0.5%, RSDs typically between 2% and 5% (for natural abundance samples the RSDs were larger at 63%), and standard deviations for absolute ^{235}U content typically between 0.2% and 0.5%.[72] To further optimize the analysis, the group performed a systematic scan of ^{235}U and ^{238}U emission lines between 280 nm and 745 nm to select the best emission lines and the best spectral windows for direct gaseous UF_6 enrichment analysis. The diagram of its experimental setup is shown in Fig. 10. Thirteen spectral window candidates were identified by screening the magnitude of the ^{235}U–^{238}U isotopic shifts and the signal-to-background ratio of the emission lines. They were then screened based on their overall accuracy in predicting the

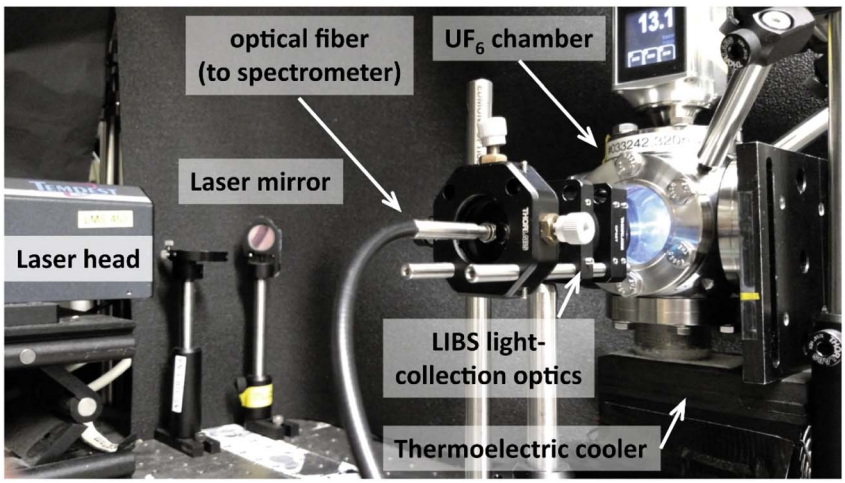

Fig. 8 Photograph showing the experimental setup and generation of laser induced plasma directly in gaseous UF_6 at a pressure of 13.1 Torr. Reproduced from ref. 71 with permission from Elsevier, copyright 2025.

^{235}U enrichment of the three UF_6 samples. The U(I) 646.498 nm emission line (with a determined ^{235}U–^{238}U isotopic shift of −17.7 pm) was found to be the best spectral window for direct UF_6 enrichment analysis. The root mean square error (RMSE) of the enrichment analysis for the three natural and low-enriched UF_6 samples was 0.31% (absolute ^{235}U content). The analytical bias and precision were better than 0.5% and 0.3%, respectively, in absolute $[^{235}U/(^{235}U + {}^{238}U)]$ ratios.[73]

The three studies collectively contribute to the development of a fast, direct, and sample-free method for the determination of U abundance in UF_6. They have progressively advanced their research, from fundamental studies of plasma properties to the search for optimal spectral windows and algorithmic optimization, and have continuously improved the precision and accuracy of the determination. However, self-absorption is still the main challenge to be overcome by the method, especially in the analysis of low-abundance samples, and further improvement of the measurement accuracy is needed. How to overcome or avoid the self-absorption problem is the key to improving the accuracy of uranium abundance testing.

5. Industrial detection of U

With the rapid development of U detection, scientists have gradually shifted the focus of their research from the laboratory to practical applications, especially in the practical application of U detection in nuclear power plants, nuclear facilities or nuclear waste disposal sites, as well as U ores in the field. In U detection in the above fields, it is difficult to complete the sampling, transport and handling processes efficiently and quickly. As a result, it is not possible to obtain U concentrations in the laboratory. Compared with laboratory detection, remote and *in situ* detection have the advantages of being more real-time, fast and convenient. It can reduce the time cost of sample transport and processing, while improving the efficiency and accuracy of detection. The practical application of remote detection and *in situ* detection in the detection of U is of great significance.

5.1. Remote detection

Remote detection means that samples can be detected at a long distance without direct contact. In environments such as nuclear power stations, nuclear facilities or nuclear waste disposal sites, direct access to samples for detection may be difficult due to radiation risks or other safety considerations. Remote detection enables safe and remote monitoring of U in these hazardous environments, ensuring the safety of operators. The efficient transmission capability of fibers along with the rapid development of femtosecond lasers has enabled the long-distance detection of LIBS. Some scientists have worked on remote detection systems, which provide technical support for remote detection of equipment in operation at nuclear power plants. Guo *et al.* independently built a remote detection system, where laser and spectral signals can be transmitted over long distances through optical fibers, so as to carry out remote LIBS detection of U in ores. They also studied the mechanism of helium's effect on U detection and improved the signal-to-noise ratio by 1.37 times. A multiple linear regression model based on the principle of the internal standard method was also proposed, which was then substituted into the partial least squares regression to improve R^2 to 0.9984, and the LOD was reduced to 142 mg kg^{-1}. The basic measurement principle is shown in Fig. 9.[74] Hartig *et al.* proposed a combination of femtosecond filament-induced laser ablation molecular and isotope spectroscopy, a method that allows long-distance laser transmission through the nonlinear process of laser filament formation. The variation rules of the emission intensity of molecules, ions and atoms with the propagation distance were investigated, and the parameters of filament distance, delay time and integration time were optimized. The relationship between the spectral intensity of U molecular spectra, the signal-to-back ratio of U atomic spectra and the filament propagation distance has been investigated. However, there is still a lack of details regarding the specific location of the characteristic spectral lines of U molecules; solving this problem is expected to achieve real-time, long-distance

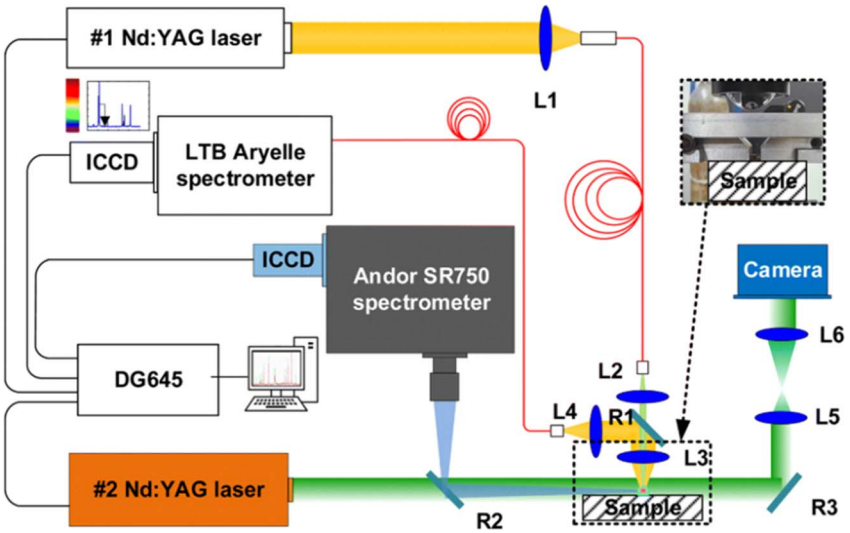

Fig. 9 Schematic of the experimental system. Reproduced from ref. 74 with permission from Royal Society of Chemistry, copyright 2025.

measurement of U; the basic principle of this method is shown in Fig. 10[75]

Up to now, remote detection systems have been applied for the detection of U, including remote LIBS detection of U ore. However, there are still some shortcomings in current remote detection. Due to the extremely high energy density and instantaneous power of femtosecond lasers, high energy excitation of samples can be performed in a very short time. This high energy excitation leads to dissociation and excitation of molecules in the sample, producing a large number of molecular spectral lines. At present, there is still a lack of detailed research on the specific wavelength of the spectral lines of U molecules, which will seriously affect the accuracy of real-time, long-range measurement of U. Secondly, the remote detection system may be affected by environmental interference and noise in practical applications, which requires further optimization of the signal-to-noise ratio and improvement of the stability of the system. In order to improve the performance of remote detection, the spectral lines of molecules reflecting U information can be further analyzed in depth. By determining the wavelengths of the spectral lines of U molecules, the accuracy and reliability of the measurement can be improved. Meanwhile, more advanced data processing algorithms and methods for optimizing parameters can be explored to improve the signal-to-noise ratio and system stability. In addition, experimental validation and engineering applications need to be strengthened to continuously improve the performance of the remote detection system to meet the needs of practical applications and to achieve rapid and accurate detection over long distances.

5.2. *In situ* detection

In situ detection methods involve carrying out the detection in the real environment in which the sample is located, without removing the sample or subjecting it to any treatment. This method provides real-time, rapid and accurate results that help to effectively monitor the presence and concentration of U, thereby helping to protect the environment and human health. In the detection of U ores in the field, *in situ* detection can help determine the amount and distribution of U in the ore. By scanning the ore, the amount of U in the ore is quickly determined. This is of great significance for mine exploration and mining, as it can improve mining efficiency and reduce the waste of resources. In addition, *in situ* detection plays an equally important role in the detection of water contaminated by nuclear weapons. By deploying portable water quality monitoring equipment around water bodies, the U concentration in water can be monitored in real time for early detection and treatment of nuclear contamination incidents, effectively protecting water resources and the ecological environment. While traditional sample collection and laboratory detection are usually time and labor intensive, *in situ* detection allows for real-time detection, saving time and costs. Based on the technical principles of spectrophotometry, fluorescence, LIBS and XRF, some scientists have developed portable or hand-held devices that are more capable of meeting the detection needs in the field. A number of scientists have already done so by adapting laboratory equipment into kits that are more responsive to the needs of field testing. Yang *et al.* used a mixture of three solid reagents, potassium bisulfate, azidoarsenic acid III and ethylene-diamine-tetraacetic acid, to react with the solution of U to form a solution to be measured with a color-developing substance. Then the absorbance of the solution was detected using a homemade hand-held spectrophotometer, and the content of U in the air could be determined according to the established standard curve, thus providing data support for the determination of the level of nuclear accidents.[76] Vibho *et al.* used Schiff base ligands to react with U(VI) to produce colored complexes and then used a low-cost LED spectrophotometer to measure the absorbance of the complexes. The team also developed a Python program for automated calibration and linearity testing and was able to directly output the

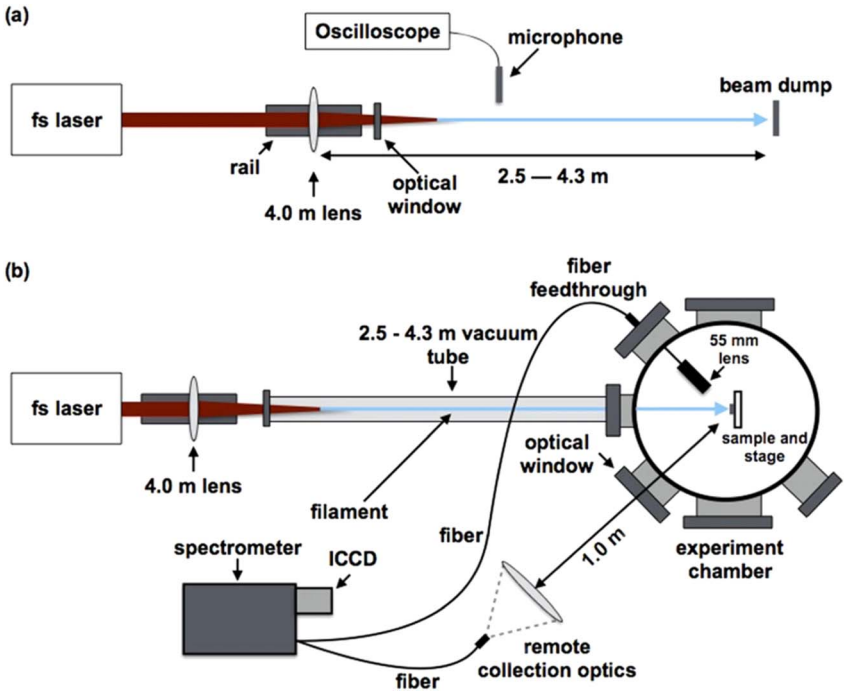

Fig. 10 (a) Filament propagation distance resolved acoustic measurement setup. (b) F2-LAMIS spectral measurement setup includes both remote collection using a fiber-coupled lens placed 1 m from the sample and a high-efficiency short focal length fiber-coupled collection optic placed 55 mm from the sample surface. Reproduced from ref. 75 with permission from Springer Nature, copyright 2025.

concentration of U in the samples, providing a more convenient and cost-effective methods of detection.[77] Chen *et al.* developed a portable liquid U content detector based on the basic measurement principle of the UV fluorescence method. And the LOD, linear range of detection and linear correlation coefficient of the instrument were 0.003 μg L^{-1}, 0.01–20 μg L^{-1} and 0.999, respectively.[78]

He *et al.* developed a laser screening device for nuclear materials, which collects spectral data through four micro-spectrometers. In addition, it uses data analysis software to automatically extract the characteristic spectral lines of U that have a high signal-to-noise ratio and are not interfered by other elements. With a LOD of around tens of ppm, the device provides strong support for real-time *in situ* detection of U ore.[79] Judge *et al.* improved the existing portable LIBS system for distinguishing between U oxide and U hydride in the assessment of U corrosion products. The sensitivity of detection of U corrosion products in different atmospheres was investigated. A data-processing application was also developed to rapidly differentiate the type and extent of U corrosion samples. The glovebox was configured to support the handheld unit as shown in Fig. 11.[80] Similarly, Manard *et al.* used hand-held laser-induced breakdown spectroscopy (HH LIBS) for rapid qualitative analysis of rare earth elements in U. Rare earth elements (Eu, Nd and Yb) were quantitatively doped into U oxide powders and analyzed by the HH LIBS instrument. This method demonstrates the ability to rapidly identify elemental constituents at sub-percent levels in a U matrix. Preliminary LODs were determined with values on the order of hundredths of a percent.[81]

In order to achieve rapid detection of U content in spent fuel reprocessing process solutions and reduce the LOD of U solutions, Fang *et al.* designed and developed an automatic hyperbolic graphite bending crystal pre-diffraction X-ray fluorescence detection system. The actual performance of the detection equipment was verified by using simulated U-containing solutions, and the LOD, quantification limit and relative standard deviation of detection for U solutions were 0.033 mg L^{-1},

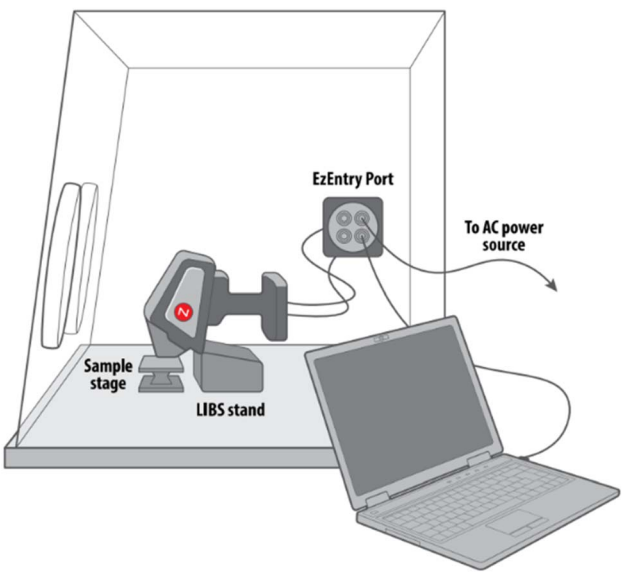

Fig. 11 Schematic of the glovebox containing a handheld LIBS system. Reproduced from ref. 80 with permission from Elsevier, copyright 2025.

0.110 mg L^{-1} and 5%, respectively.[82] Kaizer *et al.* designed an improved particle induced X-ray emission (PIXE) device for the detection of U in liquid samples. By adding barium and iridium elements as internal standards, and then using the device in combination with the internal standard method can achieve the direct and rapid detection of U content in liquid samples; it can determine as low as 10 mBq mL^{-1} in a few microliters of samples, with a measurement accuracy of about 10%.[83]

Currently, *in situ* detection has made some research progress in the field of U detection. Based on a variety of technical principles, A series of portable or hand-held devices have been developed for the detection of U in gases samples, in liquids samples and in solids samples. There are also *in situ* detection devices designed for specific scenarios, providing new ideas and technical support for the detection of nuclear materials. However, there are still some shortcomings of *in situ* detection in the field of U detection. Firstly, the sensitivity and accuracy of some devices still need to be improved, especially for the detection needs of U with low content at ppb level. Secondly, some equipment may face interference from environmental factors in field applications, which requires further optimization and improvement. In the future, there is still much to be explored in the field of U detection *in situ*. Firstly, new *in situ* detection methods can be developed to improve the sensitivity and accuracy of detection equipment to meet the detection needs of U elements in different scenarios. Secondly, the combination of *in situ* detection equipment and data analysis software can be strengthened to achieve automatic processing and analysis of data to improve detection efficiency and accuracy. By transforming the excellent detection methods in the laboratory into practical applications, the effectiveness of *in situ* detection technology can be improved to provide better support for environmental protection, resource utilization and human health.

6. Conclusion

With the rapid development of the nuclear industry, the detection of U in nuclear power plants, nuclear facilities or nuclear waste disposal sites, as well as in U ores in the field, has been emphasized. Rapid and high-precision detection of U in a variety of sample states is also an inevitable trend for the future development of the industry. The state of the sample required for different detection methods is different. A comprehensive summary of the current research on U detection shows that ICP-OES, ICP-MS, AIMS, spectrophotometry, fluorescence, and AAS can only be used for detecting liquid samples. If the sample is solid, it needs to be digested with strong acid or converted into a liquid using a buffer before detection, which is a time-consuming and complicated experimental process. However, LIBS and XRF can be used not only for the detection of powder compaction but also for the direct detection of solid samples, which imposes fewer restrictions on sample types. From this, it can be seen that LIBS and XRF are superior in terms of detection speed and ease of detection. In addition, for remote detection and *in situ* detection, LIBS, XRF, spectrophotometry, and fluorescence have portable equipment available, which can meet the needs of on-site inspection. In the future, we can consider the use of LIBS and XRF, NIRS, Raman and other multi-spectral fusion methods. Rapid detection of U content in a variety of sample states enables the rapid, stable, high-precision measurement of U content in complex samples.

Data availability

Data will be made available on request.

Conflicts of interest

The authors acknowledge that there is no conflict of interest in this article.

Acknowledgements

The authors are grateful for the financial support from the Joint Funds of the National Natural Science Foundation of China (No. 2023YFF0714901), the National Key Research and Development Program of China (No. 2023YFF0714901), the Carbon Neutrality and Energy System Transformation (CNEST) Program led by Tsinghua University, the Huaneng Group Science and Technology Research Project (No. HNKJ22-H105), and the Scientific Research in Uranium Geological Exploration Program led by China Nuclear Geology (No. D2307).

References

1 Y. C. Song, B. L. Deng, K. Wang, Y. J. Zhang, J. Gao and X. Q. Cheng, *J. Environ. Chem. Eng.*, 2024, **12**(5), 113967.
2 M. B. Andersen, T. Elliott, H. Freymuth, K. W. W. Sims, Y. L. Niu and K. A. Kelley, *Nature*, 2015, **517**, 356–U463.
3 N. Seko, A. Katakai, S. Hasegawa, M. Tamada, N. Kasai, H. Takeda, T. Sugo and K. Saito, *Nucl. Technol.*, 2003, **144**, 274–278.
4 S. S. Li, Q. Q. Zhu, J. Q. Luo, Y. Z. Shu, K. X. Guo, J. X. Xie, F. Z. Xiao and S. Y. He, *Indian J. Microbiol.*, 2021, **61**, 417–426.
5 W. Davies and W. Gray, *Talanta*, 1964, **11**, 1203–1211.
6 M. Bickel, *J. Nucl. Mater.*, 1997, **246**, 30–36.
7 K. Rogers, R. Watters, M. Holland, A. Tourville, B. Roach, C. Hexel, J. M. Giaquinto and P. Mason, *Update on the High Precision Titration Method for Uranium Assay Supported by NBL Program Office*, Oak Ridge National Lab, 2020, p. 32.
8 S. Mohajan, Y. C. Huang, N. F. Beier, M. Dyck, F. Hegmann, A. Bais and A. Hussein, *Opt Express*, 2023, **31**, 32335–32349.
9 M. Ohata, T. Kidokoro, M. Kurahashi and A. Hioki, *Bunseki Kagaku*, 2010, **59**, 903–910.
10 S. Panebianco, P. Mazzoleni, G. Barone, A. Musumarra, M. G. Pellegriti, A. Pulvirenti, A. Scordino and G. Cirvilleri, *Food Chem.*, 2022, **383**, 132364.
11 S. Pandhija and A. K. Rai, *Appl. Phys. B*, 2009, **94**, 545–552.
12 X. Z. Li, C. Xiong, K. Sun, F. Fang and Q. X. Zhang, *J. Korean Phys. Soc.*, 2021, **78**, 737–742.
13 R. K. Singhal, P. K. Sharma, M. K. T. Bassan, H. Basu and A. V. R. Reddy, *J. Radioanal. Nucl. Chem.*, 2011, **288**, 149–156.

14 M. Rezaee and F. Khalilian, *J. Radioanal. Nucl. Chem.*, 2015, **304**, 1193–1200.
15 S. F. Boulyga, J. L. Matusevich, V. P. Mironov, V. P. Kudrjashov, L. Halicz, I. Segal, J. A. McLean, A. Montaser and J. S. Becker, *J. Anal. Spectrom.*, 2002, **17**, 958–964.
16 S. Frelon, M. Monleau, E. Tourlonias, O. Delissen, V. Chazel and F. Paquet, *Can. J. Anal. Sci. Spectrosc.*, 2005, **50**, 280–288.
17 R. S. Aswal, M. Prasad, I. Dutt, A. Sharma, A. Kumar, A. Raturi, S. K. Sahoo and R. C. Ramola, *J. Radioanal. Nucl. Chem.*, 2024, **333**, 3027–3045.
18 Arti and R. Mehra, *J. Radioanal. Nucl. Chem.*, 2024, **333**, 4765–4772.
19 D. Mannion, J. Mannion, W. Kuhne and M. Wellons, *J. Am. Soc. Mass Spectrom.*, 2021, **32**(1), 8–13.
20 K. Coopersmith, R. B. Cody, J. M. Mannion, J. T. Hewitt, S. B. Koby and M. S. Wellons, *Rapid Commun. Mass Spectrom.*, 2019, **33**, 1695–1702.
21 H. M. Dion, L. K. Ackerman and H. H. Hill, *Talanta*, 2002, **57**, 1161–1171.
22 A. A. El-Sayed, M. M. Hamed, H. A. Hmmad and S. El-Reefy, *Radiochim. Acta*, 2007, **95**, 43–48.
23 M. Behpour, s. m. Ghoreishi, N. Qamsari, N. Soltani and M. Foroushani, *Chin. J. Chem.*, 2010, **28**, 1457–1462.
24 C. Mukhopadhyay, S. M, D. Sivakumar, D. Krishnan and S. R. V, *J. Radioanal. Nucl. Chem.*, 2019, **322**, 743–750.
25 A. E. Hixon, D. P. Diprete and T. A. Devol, *J. Radioanal. Nucl. Chem.*, 2013, **298**, 419–427.
26 M. Kumar, S. Suman, S. Pugazhendi, K. Dhamodharan and K. A. Venkatesan, *Talanta*, 2024, **280**, 126673.
27 S. Lehmann, G. Geipel, G. Grambole and G. Bernhard, *Spectrochim. Acta, Part A*, 2009, **73**, 902–908.
28 Z. Badr, H. Gomaa, M. S. A. El-Gaby, F. A. Faraghally, M. Taher, M. Abdelmottaleb, H. M. Ali and M. A. Abdel-Lateef, *Luminescence*, 2022, **37**, 1001–1008.
29 S. J. Xiao, A. T. Qiu, H. H. Li, M. P. Wang, L. Zhang, K. X. Guo, J. Guo and J.-D. Qiu, *Spectrochim. Acta, Part A*, 2023, **289**, 122182.
30 S. Kumar, S. Maji, M. Venkatesh, R. Ganesan and K. Sundararajan, *J. Radioanal. Nucl. Chem.*, 2020, **325**, 191–198.
31 M. Hidayath, B. S. K. Lavanya, S. N. Namitha, M. S. Chandrashekara and S. A. Pandit, *Radiat. Prot. Dosim.*, 2024, **200**, 994–1002.
32 N. Goyal, S. Thulasidas, S. Godbole and A. Spectroscopy, *At. Spectrosc.*, 2012, **33**, 123–129.
33 G. Kaur, R. Kumar, S. Mittal, P. Sahoo and U. Vaid, *Hum. Ecol. Risk Assess.*, 2019, **27**, 1–22.
34 N. Goyal, P. J. Purohit and A. G. Page, *Fresenius' J. Anal. Chem.*, 1998, **361**, 429–432.
35 N. Smječanin, M. Nuhanović, M. Preljević, J. Sulejmanović and S. Begić, *Environ. Res.*, 2024, **263**, 120034.
36 Z. S. Xu, L. Liu, Z. Q. Hao, Z. W. Deng, Y. Lu, Z. Y. Zhao, J. M. Li, J. L. Shi and X. D. He, *J. Anal. Spectrom.*, 2023, **38**, 2073–2079.
37 S. Yao, Z. Yu, Z. Hou, L. Guo, L. Zhang, H. Ding, Y. Lu, Q. Wang and Z. Wang, *TrAC, Trends Anal. Chem.*, 2024, **177**, 117795.
38 C. A. Akpovo, A. Ford and L. Johnson, *Appl. Phys. B*, 2016, **122**, 154.
39 R. C. Chinni, D. A. Cremers, L. J. Radziemski, M. Bostian and C. Navarro-Northrup, *Appl. Spectrosc.*, 2009, **63**, 1238–1250.
40 R. E. Russo, J. J. Gonzalez, D. Oropeza, C. Y. Liu, J. Chirinos and G. C. Y. Chan, *Spectrochim. Acta B*, 2024, **216**, 106928.
41 K. Mori, T. Hourai, T. Matsuyama, S. Zhuo and K. Tsuji, *Anal. Sci.*, 2024, **40**, 367–373.
42 J. Orsilli, A. Migliori, R. Padilla-Alvarez, M. Martini and A. Galli, *J. Anal. Spectrom.*, 2023, **38**, 174–185.
43 Y. Li, J. Hu, C. Li and X. Hou, *Anal. Chem.*, 2024, **96**, 5757–5762.
44 Y. Zhang, C. Q. Fu, J. Qiu, J. H. Qu, Y. C. Yang, B. Tang and R. B. Wang, *Appl. Radiat. Isot.*, 2024, **210**, 111367.
45 T. Matsuyama, Y. Izumoto, H. Imaseki, T. Hamano, Y. Sakai and H. Yoshii, *J. Nucl. Sci. Technol.*, 2017, **54**, 940–943.
46 Y. Izumoto, T. Matsuyama, K. Ishii, Y. Sakai, Y. Oguri and H. Yoshii, *X Ray Spectrom.*, 2019, 438–442.
47 H. Takahashi, Y. Izumoto, T. Matsuyama and H. Yoshii, *X Ray Spectrom.*, 2019, **48**, 366–374.
48 H. Yoshii, K. Takamura, T. Uwatoko and Y. Sakai, *Membranes*, 2023, **13**, 299.
49 N. Varnava and I. Pashalidis, *J. Radioanal. Nucl. Chem.*, 2024, **333**, 1083–1088.
50 M. Almeshari, Y. Alzamil, H. Alahmad, K. Alenazi, A. Alhammad and A. El-Taher, *J. Radioanal. Nucl. Chem.*, 2024, 6311–6318.
51 P. A. Greene, C. L. Copper, D. E. Berv, J. D. Ramsey and G. E. Collins, *Talanta*, 2005, **66**, 961–966.
52 A. Boryło, W. Nowicki, G. Olszewski and B. Skwarzec, *J. Environ. Sci. Health, Part A: Toxic/Hazard. Subst. Environ. Eng.*, 2012, **47**, 1831–1842.
53 E. D. Hoegg, B. T. Manard, E. M. Wylie, K. J. Mathew, C. F. Ottenfeld and R. K. E. m. M. C. E. Marcus, *J. Am. Soc. Mass Spectrom.*, 2019, **30**, 278–288.
54 S. Bowden, K. M. Samperton, E. D. LaBone, H. B. Lawton, A. M. Waldron, J. M. Mannion, M. S. Wellons and D. R. Mannion, *J. Anal. Spectrom.*, 2025, **40**, 195–201.
55 D. A. Galson, B. P. Atkin, P. K. Harvey and H. W. Zhang, *Overseas Uranium Geology*, 1984, pp. 97–101.
56 J. Ji, W. Song, Z. Hou, L. Li, X. Yu and Z. Wang, *Anal. Chim. Acta*, 2022, **1235**, 340551.
57 Q. Li, W. Zhang, Z. Tang, R. Zhou, J. Yan, C. Zhu, K. Liu, X. Li and X. Zeng, *J. Anal. Spectrom.*, 2020, **35**, 626–631.
58 Z. W. Zhang, R. Qiu, Y. X. Yao, Q. Wan, G. W. Pan and J. F. Shi, *Spectrosc. Spectral Anal.*, 2023, **43**, 57–61.
59 B. T. Manard, C. D. Quarles, V. C. Bradley, T. L. Spano, N. A. Zirakparvar, B. W. Ticknor, D. R. Dunlap, P. Cable-Dunlap, C. R. Hexel and H. B. Andrews, *J. Am. Chem. Soc.*, 2024, **146**, 14856–14863.
60 Z. Q. Hao, K. Liu, Q. L. Lian, W. R. Song, Z. Y. Hou, R. Zhang, Q. Q. Wang, C. Sun, X. Y. Li and Z. Wang, *Front. Phys.*, 2024, **19**, 62501.

61 S.-K. Han, S.-H. Park and S.-K. Ahn, *Plasma Sci. Technol.*, 2020, **22**, 074015.
62 X. Mao, G. C. Y. Chan, I. Choi, V. Zorba and R. E. Russo, *J. Radioanal. Nucl. Chem.*, 2017, **312**, 121–131.
63 P. Fan, S. Ren, L. Gong, X. Meng, X. Liu, B. Jiao, S. Sun and X. Guo, *Appl. Phys. B*, 2024, **130**, 86.
64 T. B. Adimedha, R. A. Farrenzo, I. G. Sukadana, R. D. Nugraheni, F. Pratiwi, R. C. Ciputra, F. D. Indrastomo, H. Syaeful and Y. Rachael, *Eksplorium-Buletin Pusat Teknologi Bahan Galian Nuklir*, 2024, **45**, 1–16.
65 I. Choi, G. C. Y. Chan, X. Mao, D. L. Perry and R. E. Russo, *Appl. Spectrosc.*, 2013, **67**, 1275–1284.
66 P. K. Morgan, J. R. Scott and I. Jovanovic, *Spectrochim. Acta, Part B*, 2016, **116**, 58–62.
67 D. Zhang, X. Ma, S. Wang and X.-L. Zhu, *Plasma Sci. Technol.*, 2015, **17**, 971–974.
68 L. Liu, S. Li, X. Huang, Y. Lu, K. Chen, R. Pik, L. Jiang, J. F. Silvain and Y. F. Lu, *J. Anal. Spectrom.*, 2015, **30**, 1128–1132.
69 M. Holá, K. Novotný, J. Dobeš, I. Krempl, V. Wertich, J. Mozola, M. Kubeš, V. Faltusová, J. Leichmann and V. Kanický, *Spectrochim. Acta, Part B*, 2021, **186**, 106312.
70 H. B. Andrews, C. Derrick Quarles, V. C. Bradley, T. L. Spano, J. A. Petrus, B. Paul, N. Alex Zirakparvar, D. R. Dunlap, C. R. Hexel and B. T. Manard, *Microchem. J.*, 2024, **196**, 109605.
71 G. C. Y. Chan, L. R. Martin, L. D. Trowbridge, Z. Zhu, X. Mao and R. E. Russo, *Spectrochim. Acta, Part B*, 2021, **176**, 106036.
72 G. C. Y. Chan, X. Mao, L. R. Martin, L. D. Trowbridge and R. E. Russo, *J. Radioanal. Nucl. Chem.*, 2022, **331**, 1409–1421.
73 G. C. Y. Chan, L. R. Martin and R. E. Russo, *Appl. Spectrosc.*, 2022, **77**, 819–834.
74 X. Guo, J. Wu, J. Li, M. Shi, X. Zhu, Y. Zhou, D. Wu, Z. Song, S. Huang and X. Li, *J. Anal. Spectrom.*, 2024, **39**, 2716–2727.
75 K. C. Hartig, I. Ghebregziabher and I. Jovanovic, *Sci. Rep.*, 2017, **7**, 43852.
76 Y. Yang, S. Xiao, Y. Zhang, L. Huang and Q. Liu, *Anal. Methods*, 2013, **5**, 4785–4789.
77 A. Vibho, C. Rogat, E. Karavas, R. Mohammed, P. Ogadi, M. White, T. Salois, C. Anderson, M. W. Prairie, S. H. Frisbie and S. K. Gallant, *PLoS One*, 2024, **19**, e0308516.
78 S. H. Chen, L. T. Wang, M. M. Gong, H. Y. Ding, Q. W. Huang and Z. M. Du, *Chin. J. Anal. Chem.*, 2023, **51**, 1414–1422.
79 Y. He, F. M. Hu, Z. X. Gao, S. Z. Zhang and J. Li, Identification of nuclear materials using portable Laser-induced Plasma Spectroscopy, *Optical Spectroscopy and Imaging; and Atmospheric and Environmental Optics*, 2023.
80 E. J. Judge, K. Campbell and D. Kelly, *Spectrochim. Acta, Part B*, 2021, **186**, 106325.
81 B. T. Manard, E. M. Wylie and S. P. Willson, *Appl. Spectrosc.*, 2018, **72**, 1653–1660.
82 Y. T. Fang, Z. Q. Wang, Q. W. Liu, M. Wu, J. Ma and Y. Q. Qin, *At. Energy Sci. Technol.*, 2024, **58**, 721–730.
83 J. Kaizer, M. Ješkovský, J. Pánik, J. Zeman, S. Dulanská, B. Horváthová and P. P. Povinec, *J. Radioanal. Nucl. Chem.*, 2018, **318**, 591–597.